PCCP

ROYAL SOCIETY OF CHEMISTRY

PAPER

View Article Online
View Journal

Cite this: DOI: 10.1039/d5cp02069g

Properties of CB7CB-D_4 as derived from ^{129}Xe and ^{2}H NMR experiments and computations

Jukka Jokisaari * and Juha Vaara

Twist-bend nematic liquid crystal phases are fundamentally interesting as chiral macroscopic structures arising from achiral molecules, as well as from the perspectives of photonics and switching applications. Conical angle and orientational order are the key properties of the twist-bend nematic phase. In the present case, we investigate the conical angle in 1″,7″-bis(4-cyanobiphenyl-4′-yl)heptane (CB7CB), which displays ordinary nematic (N) and twist-bend nematic (N_{TB}) phases, utilizing ^{129}Xe shielding and ^{2}H quadrupole splitting in CB7CB-D_4. When applying the ^{129}Xe shielding, measured with respect to an external gaseous xenon sample, the bulk susceptibility effect must be considered. For this purpose, the diamagnetic susceptibility tensor was computed. The analysis of the ^{2}H NMR data necessitates the knowledge of the ^{2}H quadrupole coupling tensor element along the C–D bond. Computations and data analyses show that the commonly used value of 168 kHz is slightly underestimated. Another property investigated is the temperature dependence of the ^{129}Xe linewidth ($\nu_{1/2}$). It reveals two things: (i) when approaching the phase transitions from the high-temperature side, $\nu_{1/2}$ increases abruptly, but decays, after the transition, exponentially toward the values in the isotropic phase, and (ii) upon cooling under *ca.* 355 K in the N_{TB} phase, $\nu_{1/2}$ increases exponentially. Subtraction of the linewidth distributions at the phase transitions reveals that $\nu_{1/2}$ remains independent of temperature in the isotropic and nematic phases, and partially also in the twist-bend nematic phase. The assumption that the ^{129}Xe linewidth reveals the T_2 relaxation rate, $1/T_2$, leads to the conclusion that the rate is independent of temperature in the isotropic and nematic phases and partially also in the twist-bend nematic phase.

Received 2nd June 2025,
Accepted 13th November 2025

DOI: 10.1039/d5cp02069g

rsc.li/pccp

Introduction

The discovery and experimental verification of the twist-bend nematic (N_{TB}) phase are some of the most important developments in the field of liquid crystals. It reveals the fundamental physics of liquid crystals, provides insight into molecular self-organization, and opens technological opportunities in fast electro-optic and photonic applications. As described by Dunmur,[1] this led about 15 years ago to great interest among liquid crystal scientists. The most studied compound, displaying the conventional nematic (N) phase and the twist-bend nematic phase, is 1″,7″-bis(4-cyanobiphenyl-4′-yl)heptane (CB7CB). Although the properties of the twist-bend nematic phase in CB7CB have been extensively investigated, there remains uncertainty about the temperature dependence of the conical angle between the helical axis and the liquid crystal director.

^{129}Xe NMR of dissolved xenon gas has appeared as a powerful method for the determination of various properties of liquid crystals. Xenon has two NMR active isotopes, ^{129}Xe and ^{131}Xe. The former possesses a spin of 1/2 while the latter has a spin of 3/2, *i.e.*, it is quadrupolar. Both isotopes have a relatively high natural abundance, which in this respect is quite favourable for NMR studies. However, detection of ^{131}Xe NMR is demanding because of its short T_2 relaxation time, resulting in a broad linewidth. Furthermore, the spectral intensity is distributed between three lines in the solid and liquid crystal phases. In the case where experiments are successful in these phases, ^{131}Xe NMR spectra reveal a property not available *via* ^{129}Xe NMR, which is the electric field gradient (EFG) at the nuclear site created by the environment and deformation of the electron distribution of the atom.[2] Comparison of ^{129}Xe and ^{131}Xe shielding in the same liquid crystalline environment reveals the biaxiality of the environment.[3–5] This is based on the second-order quadrupole shift (SOQS) in the ^{131}Xe spectra. ^{129}Xe NMR of a liquid crystal solution can be used to extract a lot of versatile information such as temperature dependence of the orientational order parameter,[6] phase transitions,[7] temperature dependence of the solvent density (isobaric thermal expansion coefficient),[8] the sign of the diamagnetic anisotropy,[9] the occurrence of induced smectic phases,[10] the anisotropy of the ^{129}Xe shielding tensor due to the deformation of the electron cloud,[8] and the temperature dependence of the conical (tilt) angle in chiral smectic and twist-bend nematic phases.[6] The conical angle and the orientational order

NMR Research Unit, University of Oulu, P.O. Box 3000, FI-90014, Finland.
E-mail: jukka.jokisaari@oulu.fi

parameter are the key properties of the twist-bend nematic phase in CB7CB. Therefore, it is most important that these properties are known as accurately as possible. Earlier investigations have reported a large scatter of the conical angle values, applying different methods.[11,12]

In the present work, we first concentrate on the methods based on ^{129}Xe NMR of xenon dissolved in CB7CB-D_4 on the one hand, and on the utilization of the ^{2}H quadrupolar splitting in the determination of the conical angle, on the other hand. Moreover, we discuss another property of ^{129}Xe NMR which reveals valuable information about the liquid crystal used as the solvent. This property is the linewidth, full width at half height, for which $\nu_{1/2}$ will be used as a symbol, detected as a function of temperature.

Experimental

^{129}Xe NMR experiments were performed in CB7CB-D_4 (see Fig. 1). The solubility of xenon in CB7CB is not known but utilizing typical values one can estimate that the mole concentration of Xe in CB7CB is *ca.* 1 mol%. The transition temperatures for CB7CB doped with xenon are 387.1 ± 0.5 K and 374.4 ± 0.5 K for the N–I and N_{TB}–N transitions, respectively; these are 2.2 and 2.3 K lower than those for the pure compound, where there is no xenon.

Details of the synthesis and NMR measurements are described, for example, in ref. 6. The ^{129}Xe shielding in CB7CB-D_4 was referenced to the value of external gaseous ^{129}Xe, which was considered independent of the temperature. However, when experiments are carried out in different environments, it is necessary to consider the difference in the diamagnetic susceptibilities of the environments. This will be discussed in the next section. The ^{2}H NMR data were originally reported in ref. 12 and were used in ref. 6, as well.

Computations

In the present case, the ^{129}Xe NMR shielding was measured relative to the respective signal of an external gaseous sample. In such a case, the effect of bulk susceptibility must be considered. This, however, requires the knowledge of the diamagnetic susceptibility tensor (DST) of CB7CB, and that of the xenon gas. Unfortunately, no information on the full DST could be found in the literature. The diamagnetic properties of CB7CB are often claimed to be similar to those of 5CB.[14] The calculations carried out here do not quite agree with this.

Quantum-chemical calculations were carried out using density-functional theory (DFT) for DST and ^{2}H quadrupole coupling constant of the CB7CB molecule. The first two properties were, for comparison, also calculated for the Xe atom and for the 5CB molecule. First, the geometries of the CB7CB and 5CB molecules were optimised *in vacuo*, in an all-*trans* configuration, using the PBE0 exchange–correlation functional[15] and the def2-TZVP basis set[16] on the Turbomole software.[17] The semiempirical D4 dispersion correction[18] was applied. The optimised geometries are provided in the SI. The ^{2}H quadrupole coupling constants were obtained for the –CD_2 groups next to the innermost phenyl rings, in the optimised geometry, using similar methodology to that applied for optimising the geometry. Additionally, a locally dense basis set with the def2-QZVPPD basis set[19] was applied on these groups, while the rest of the system was treated with the def2-TZVP basis set.

The DST calculations were done on all the three systems at the optimised geometry at the PBE0/def2-TZVP level on the Gaussian 16 programme.[20]

The results of the molecular property calculations are given in Table 1. In fact, instead of DST, the related single-molecular property which is calculated is the molecular magnetizability ξ, from which an estimate of the susceptibility of a medium consisting of such molecules can be obtained as $\chi = \mu_0 N_A \xi$.[22] The DST is typically well-reproduced by DFT with the present, triple-zeta level basis set, and the data should be representative of a molecule *in vacuo*, at the equilibrium geometry. It can be noted that, as an extensive molecular property, the isotropic susceptibility $\chi_{iso} = -3.83 \times 10^{-9}$ m^3 mol^{-1} is roughly doubled in value in CB7CB as compared to 5CB, which is in line with the molecular structures in question.

The value of the susceptibility anisotropy $\Delta\chi = \chi_{cc} - (\chi_{aa} - \chi_{bb})$ depends on the molecular frame (a, b, c) that is chosen to represent the tensor. The 5CB molecule forms uniaxial liquid crystal phases and, in the case of a positive susceptibility anisotropy such as in the present case, the relevant reference direction c is aligned with the mechanical long axis of the molecule, *i.e.*, the principal axis of the moment of inertia $\boldsymbol{I}$ tensor that corresponds to the minimum eigenvalue of $\boldsymbol{I}$. In 5CB, this coincides well with the direction from the terminal N atom on one end of the molecule with the carbon atom of the terminal –CH_3 group, at the other end. This direction is aligned with the principal axis corresponding to the middle eigenvalue of the $\boldsymbol{\chi}$ tensor, $\chi_{cc} = -1.79 \times 10^{-9}$ m^3 mol^{-1}, with the two other eigenvalues equal to $\chi_{aa} = -3.01 \times 10^{-9}$ and $\chi_{bb} = -1.71 \times 10^{-9}$ in the same units. Even though $\boldsymbol{I}$ is nearly cylindrically symmetric in 5CB, the molar susceptibility tensor is noted to have a substantial asymmetry. The reason is the very strong axiality of the local DST tensors of the two phenyl groups of 5CB, each with unique axes that are perpendicular to the plane of the phenyl groups, residing perpendicular also to the long axis of the entire 5CB molecule. The normal vectors of the two phenyl groups are at an angle of about 37 degrees in the optimised molecular geometry, hence their susceptibilities reinforce each other and produce the strong asymmetry of $\boldsymbol{\chi}$. However, the molecules are expected to undergo, in the NMR time scale, rapid rotation around the long axis of $\boldsymbol{I}$, which renders the time average susceptibility cylindrically symmetric around that axis. The presently calculated anisotropy

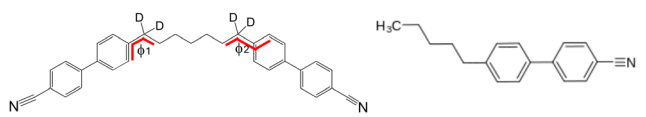

Fig. 1 Structure of CB7CB-D_4 (left) and 5CB (right). For CB7CB, the two dihedral angles ϕ_1 and ϕ_2, used in rotational averaging of the quantum-chemically calculated diamagnetic susceptibility tensor, are indicated.

Table 1 Quantum-chemically calculated molar magnetic susceptibility and ^{2}H nuclear quadrupole coupling constant. The PBE0/def2-TZVP level of theory was used, unless otherwise specified

Property	Symbol and unit	System		
		Xe	5CB	CB7CB
Magnetizability	ξ_{iso} (10^{-30} J T^{-2})	−824	−2870	−5060
Magnetizability anisotropy[a]	$\Delta\xi$ (10^{-30} J T^{-2})	—	674	13.3
Magnetizability[b]	ξ_{iso} (10^{-30} J T^{-2})	—	—	−5110
Magnetizability anisotropy[a,b]	$\Delta\xi$ (10^{-30} J T^{-2})	—	—	520
Molar susceptibility[c]	χ_{iso} (10^{-9} m^3 mol^{-1})	−0.62	−2.17	−3.83
Molar susceptibility anisotropy[a,c]	$\Delta\chi$ (10^{-9} m^3 mol^{-1})	—	0.57 (0.53[d])	0.01
Molar susceptibility[b]	χ_{iso} (10^{-9} m^3 mol^{-1})	—	—	−3.86
Molar susceptibility anisotropy[a,b]	$\Delta\chi$ (10^{-9} m^3 mol^{-1})	—	—	0.39 (0.86[e])
^{2}H electric field gradient[f]	^{2}H V_{zz} (a.u.)	—	—	−0.291 (−0.275)
^{2}H quadrupole coupling constant[e]	^{2}H q_{CD} (kHz)	—	—	−195 (−185)

[a] Anisotropies in the principal axis frame of the moment of inertia tensor $\boldsymbol{I}$, $\Delta P = P_{33} - (P_{11} + P_{22})/2$, where the tensor component P_{33} is aligned with the long axis of $\boldsymbol{I}$. [b] Extrapolated value taking into account conformational averaging according to eqn (1). [c] An estimate of the molar susceptibility of the medium is obtained from the calculated single-molecular magnetizability, assuming simple scaling with the number density of the medium. [d] Experimental value from ref. 23. [e] Experimental value from ref. 21. [f] Average over the four CD_2-group deuteron nuclei. Figures in parentheses with the locally dense basis set applied on the groups in question (see the text).

resulting for 5CB from this choice of coordinate frame, $\Delta\chi$ = 0.57 × 10^{-9} m^3 mol^{-1}, is in excellent agreement with the experimental value of 0.53 × 10^{-9} m^3 mol^{-1} from ref. 23. This success serves as a sanity check of both (1) the underlying DFT methodology applied at the single-molecular level and (2) the assumption that the DST, a material property, additively consists of the single-molecular properties.

The situation is more complicated for the V-shaped CB7CB molecule. There is a clearly defined cylindrical axis of $\boldsymbol{I}$ also in this case, coinciding with the internuclear axis between the terminal nitrogen atoms in the optimised geometry. Calculating $\Delta\chi$ using the mechanical long axis of the molecule as the reference direction gives practically a zero result at the equilibrium geometry, which would imply vanishing orientational bias and contradicts the existence of the N phase with the director aligned with the external magnetic field. However, the value of $\Delta\chi$ is very sensitive to the molecular conformation. Referenced to the optimised structure, a metastable conformer at +0.93 kcal mol^{-1} can be reached by rotating one of the biphenyl moieties by 90 degrees around the bond joining the inner phenyl group with respect to the first –CH_2 group. In this metastable conformer, using the mechanical long axis of the molecule as the reference direction, one obtains the result $\Delta\chi$ = 0.63 × 10^{-9} m^3 mol^{-1}.

It is apparent that, to obtain meaningful data for the analysis of experiments, one must perform conformational averaging in the case of CB7CB. To this end, we carried out a relaxed two-dimensional scan over the two dihedral angles, marked in Fig. 1, that join the two biphenyl moieties to the aliphatic chain at the centre of the molecule. This scan was carried out on the ORCA software,[24] using DFT with the PBE exchange–correlation functional,[25] the def2-SVP basis[16] and the D4 dispersion correction. The dihedral angles were fixed to values in a two-dimensional grid ranging from 90 to 420 degrees in 30-degree intervals, and all the other degrees of freedom were optimised for minimum energy, at each of the grid points. At the global energy minimum obtained at the PBE/def2-SVP level of theory, the isotropic molar susceptibility and susceptibility anisotropy (the latter with reference to the mechanical long axis of the molecule) gained the values of −3.87 and 0.00, respectively, in units of 10^{-9} m^3 mol^{-1}. There is only a small change as compared to the PBE0/def2-TZVP equilibrium-geometry data, −3.83 and 0.01, respectively, in the same units. The Boltzmann-weighted average (at 300 K temperature) over the total of 144 points in the relaxed 2-dimensional scan resulted in the averages χ_{iso} = −3.90 and $\Delta\chi$ = 0.39 × 10^{-9} m^3 mol^{-1}. Hence, we arrive at our best estimates, in Table 1, by extrapolating both the isotropic susceptibility and its anisotropy as

$$P_{ext} = \left(P^{eq}_{PBE0/TZVP} - P^{eq}_{PBE/SVP}\right) + \langle P^{scan}_{PBE/SVP}\rangle^{300K}_{conf}. \quad (1)$$

Here, P_{ext} is the extrapolated quantity, P_x denotes the property calculation at level x, eq refers to the optimised equilibrium geometry, scan refers to the points of the two-dimensional grid, and $\langle\ \rangle^T_{conf}$ refers to Boltzmann averaging over molecular conformations at temperature T. This resulted in χ_{iso} = −3.86 and $\Delta\chi$ = 0.39 × 10^{-9} m^3 mol^{-1}. In general, the isotropic susceptibility is hardly affected by the conformation of the system, whereas the susceptibility anisotropy is quite sensitive to it. The scan data used in eqn (1) are included in the SI. In particular, our result for $\Delta\chi$ in CB7CB is of the same positive sign and order of magnitude, but less than half of the magnitude of that obtained in ref. 21 from their Frederiks effect measurements, $\Delta\chi_0$ = 0.86 × 10^{-9} m^3 mol^{-1}. The experimental anisotropy results indirectly from an optical experiment, and the isotropic χ is not reported in ref. 21. While our calculations address directly both these quantities (under the approximation of additivity), it is not ruled out that a more detailed intra- and intermolecular dynamics modelling, than what is carried out presently, would be necessary for an entirely quantitative prediction of this parameter. We performed the susceptibility correction of the ^{129}Xe NMR shift both using the presently calculated $\Delta\chi$ and that mentioned in ref. 21.

Deuterium quadrupole coupling is particularly sensitive to the basis set,[26] and we see a significant reduction of 10 kHz in the value of q from the result at the triple-zeta level to the quadruple-zeta level. Additionally, the sensitivity to the CD bond length shows in the (ro)vibrational corrections to this

quantity, which in earlier studies have been placed at −3% for the methyl halides (CD_3X, X = F–I),[26] corresponding in the present case to about −5.5 kHz of further change of q, and about −10 kHz for deuterated benzenes.[27] The third factor influencing q would come from intermolecular effects and solvation, with the largest potential changes arising from hydrogen bonding with the solvent molecules. This is not a very likely mechanism for the CD_2 groups in the present liquid crystal system. Hence, combining the calculated q with the locally dense basis set with an average of the internal motion corrections in the two above-mentioned example cases leads to 177 kHz as our current best estimate for the ^{2}H quadrupole coupling constant of the CB7CB-D_4 system.

For the derivation of the conical angle from the ^{2}H quadrupolar splittings, the element of the quadrupolar coupling tensor, q_{CD}, along the C–D bond (see Fig. 1) should be known. In many cases, q_{CD} is assumed to be 168 kHz.[6,12,13,28,29]

Results

^{129}Xe shielding and conical angle

Fig. 2 shows the stack plot of the ^{129}Xe NMR spectra in CB7CB-D_4 at variable temperatures. The I–N and N–N_{TB} phase transitions are clearly visible. Interestingly, at the N–N_{TB} transition, a coexistence of the peaks arising from both the N and N_{TB} phases is observed.

The figure shows the temperature dependence of ^{129}Xe shielding (relative to that of xenon gas at room temperature and 2 atm pressure) for xenon dissolved in CB7CB-D_4. The clear jumps of the shielding at the phase transitions facilitate two conclusions: (i) the large jump at the I–N transition toward a more negative value proves that the diamagnetic anisotropy is positive and, consequently, the director and, in the twist-bend nematic phase, the helical axis orient parallel to the external magnetic field and (ii) the smaller jump at the N–N_{TB} transition originates from the onset of the tilt of the director relative to the external field.

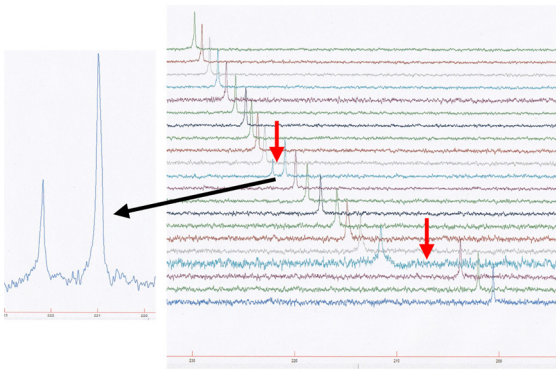

Fig. 2 Stack plot of the ^{129}Xe NMR spectra in CB7CB-D_4. Phase transition points are indicated by red arrows. Temperature increases from top to bottom, and the range of 356.8–398.6 K is shown. On the left is shown the expanded coexistence of the peaks (at 374.4 K) originating from the N (right peak) and N_{TB} (left peak) phases. At the I–N transition, the ^{129}Xe shielding jumps by 8 ppm while at the N–N_{TB} transition the jump is 1.2 ppm.

The bulk susceptibility contribution to the ^{129}Xe shielding, for a long cylindrical sample with its axis parallel with the external magnetic field, is obtained as[30]

$$\sigma_b = -\frac{1}{3}\left[\chi + \frac{2}{3}\Delta\chi P_2(\cos\theta)S\right]\frac{\rho}{M}, \quad (2)$$

where χ and $\Delta\chi$ are one-third of the trace of the DST and its anisotropy, respectively, the former being negative and the latter positive, S is the orientational order parameter, ρ is density and M is molar mass (0.454 kg mol^{-1} for CB7CB and 0.131 kg mol^{-1} for xenon). P_2 is the second Legendre polynomial and θ the conical angle. The calculated diamagnetic properties of CB7CB, χ and $\Delta\chi$, are listed in Table 1 [we are using the values extrapolated as in eqn (1)]. The orientational order parameter is modelled by the Haller function[31]

$$S(T) = \left(1 - y\frac{T}{T_{PT}}\right)^z, \quad (3)$$

where T_{PT} is either the I–N or N–N_{TB} phase transition temperature, and y and z are adjustable parameters. The temperature dependence of the density is described by

$$\rho(T) = \rho_0[1 - \alpha(T - T_0)], \quad (4)$$

where ρ_0 is the density (1009.5 kg m^{-3} for CB7CB, 5.46 kg m^{-3} for xenon) at the reference temperature T_0 and α is the isobaric thermal expansion coefficient. The data used in estimating the bulk susceptibility effect on ^{129}Xe shielding in gas and in the CB7CB-D_4 solution are shown in Table 2.

The dependence of the ^{129}Xe shielding in a uniaxial nematic phase on the temperature and orientational order can be modelled with the function[32,33]

$$\langle\sigma_{ZZ}(T)\rangle = \sigma_0 + \sigma_d[1 - (\alpha + \tau)(T - T_0)] + \frac{2}{3}\Delta\sigma_d[1 - (\alpha + \Delta\tau)(T - T_0)]P_2(\cos\theta)S(T). \quad (5)$$

$\langle\sigma_{ZZ}(T)\rangle$ is the average of the ^{129}Xe shielding tensor element along the external magnetic field (parallel to the Z axis). The factors σ_d and $\Delta\sigma_d$ are the isotropic shielding and shielding anisotropy, respectively, at the reference temperature. The coefficients τ and $\Delta\tau$ consider the possible direct effect of temperature on the shielding and shielding anisotropy, respectively. P_2 is the second Legendre polynomial, and θ is the conical angle. Least-squares fit of function (5) to the experimental shielding values (without susceptibility

Table 2 Parameters used in the calculation of susceptibility corrections to the ^{129}Xe shielding in the phases of CB7CB

Isotropic phase	$(\alpha + \tau) = 0.0014$ K^{-1}
Nematic phase	$(\alpha + \tau) = 0.0014$ K^{-1}, $(\alpha + \Delta\tau) = -0.0018$ K^{-1}, $y = 0.998$, $z = 0.245$, $T_0 = 387.1$ K
Twist-bend	$(\alpha + \tau) = 0.0160$ K^{-1}, $(\alpha + \Delta\tau) = -0.0020$ K^{-1}, $y = 0.998$, $z = 0.245$, $T_0 = 374.4$ K
Nematic phase	$\theta(T) = 40.4^\circ\left(1 - 0.998 \times \frac{T}{374.4\ \text{K}}\right)^{0.227}$

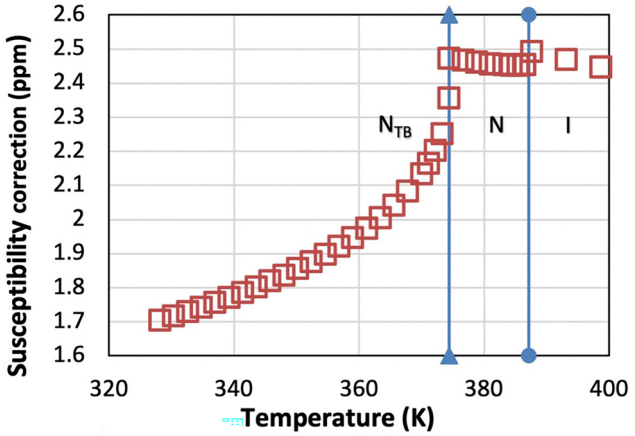

Fig. 3 Bulk susceptibility correction to the ^{129}Xe shielding in the phases of CB7CB-D_4 liquid crystal. The vertical lines indicate phase transitions.

correction) reveals the parameters y, z, $(\alpha + \tau)$, $(\alpha + \Delta\tau)$ and the conical angle, necessary for calculating the susceptibility corrections. The values are listed in Table 2.

Application of eqn (2) to xenon gas ($S = 0$, $\Delta\chi = 0$) results in $\sigma_b = 0.0086$ ppm. As mentioned in ref. 34, the temperature effect is negligible. The bulk shielding correction (including that of xenon gas) for the ^{129}Xe shielding in CB7CB-D_4 is shown in Fig. 3. The temperature dependence of the ^{129}Xe shielding without and with bulk correction in CB7CB is shown in Fig. 4, together with the least-squares fit of function (5) to the ^{129}Xe shielding corrected for the bulk susceptibility.

The fit to the susceptibility-corrected ^{129}Xe shielding also reveals the change in the temperature dependence of the conical angle. Fig. 5 shows the conical angle derived from the uncorrected and corrected ^{129}Xe shielding, together with the conical angle determined from two earlier birefringence measurements.

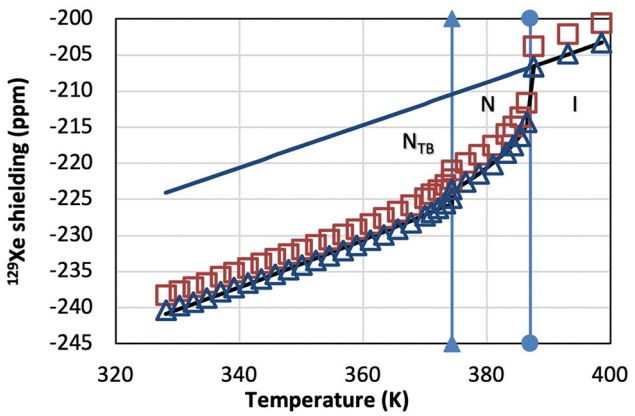

Fig. 4 ^{129}Xe shielding as a function of temperature in CB7CB-D_4 without (red squares) and with (blue triangles) bulk susceptibility correction. The solid lines show extrapolation from the isotropic phase to the liquid crystal phases (upper line) and the least-squares fit of function (5) to the susceptibility corrected ^{129}Xe shielding (lower line). The vertical lines indicate phase transitions.

The temperature dependence of the conical angle after bulk susceptibility correction to ^{129}Xe shielding obeys the equation

$$\theta(T) = 44.49 \times \left(1 - 0.998 \times \frac{T}{T_{N-N_{TB}}}\right)^{0.2235}, \qquad (6)$$

where the phase transition temperature $T_{N-N_{TB}} = 374.4$ K. The susceptibility correction was calculated also using the isotropic χ value computed in this work and $\Delta\chi$ determined in ref. 21. Consequently, as compared to using the presently calculated values for both of these parameters, the susceptibility correction increases on average by about 0.1 ppm in the N_{TB} phase, and the coefficient and exponent in eqn (6) change slightly. However, the two curves would not be distinguishable in Fig. 5. Interestingly, the conical angles derived from two birefringence measurements differ significantly.[35,36] Ref. 35 explains that the difference is due to the choice of the region from where the birefringence measurements were taken. The present data derived from the susceptibility-corrected ^{129}Xe shielding agree with the conical angle reported in ref. 35.

^{2}H quadrupole coupling and conical angle

The ^{2}H NMR spectrum of CB7CB-D_4 displays a single doublet in the conventional nematic phase. In the chiral twist-bend nematic phase, the ^{2}H NMR spectrum shows two doublets due to the prochiral deuterons. In the nematic phase, the quadrupole splitting and, in the twist-bend nematic phase, the mean of the two splittings can be presented as follows:[6]

$$|\Delta\nu| = \frac{3}{2} q_{CD} \left| P_2(\cos\gamma) P_2[\cos\theta(T)] S_p(T) \right|, \qquad (7)$$

where q_{CD} is the element of the ^{2}H quadrupolar coupling tensor along the C–D bond, P_2 is the second Legendre polynomial, γ is the angle between the C–D bond and the *para*-axis of the biphenyl fragment, $\theta(T)$ is the conical angle, and $S_p(T)$, modelled by the Haller function as in the case of the ^{129}Xe analysis, is the orientational order parameter of the *para*-axis of the biphenyl

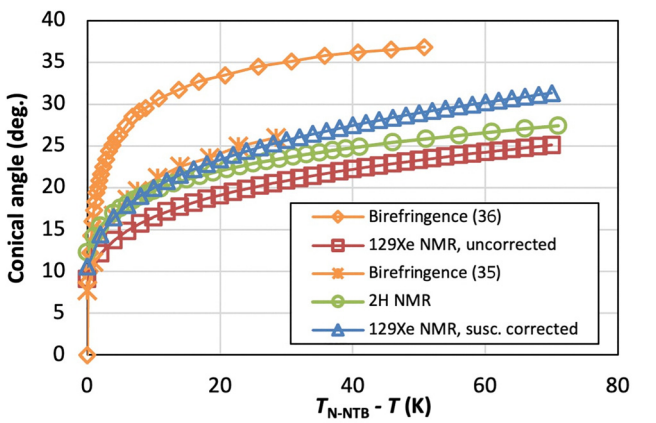

Fig. 5 Conical angle in CB7CB-D_4 as a function of temperature before (red squares) and after (blue triangles) bulk susceptibility correction to ^{129}Xe shielding, and the conical angle derived from the ^{2}H quadrupole splittings (cyan triangles). For comparison, also two results derived from birefringence measurements are shown (ref. 35 and 36).

fragment relative to the director. It is generally assumed that the C–D bond forms the tetrahedral angle with the *para*-axis.[6,12,13,26,27] The application of eqn (7) assumes that the orientational order of the biphenyl fragment can be described by a single parameter. Ref. 37, however, proves that the biaxiality order parameter is about 7.3% of the order parameter along the *para*-axis in the nematic phase and about 3.6% in the N_{TB} phase. Furthermore, as mentioned above, it is generally assumed that q_{CD} equals 168 kHz. Our computations and data analysis, however, show that it should be around 176–178 kHz, as discussed above.

We apply eqn (7) in the N_{TB} phase with keeping γ fixed to 109.6° as derived from the optimised geometry and allowing q_{CD} to change in the least-squares fit. The fit resulted in q_{CD} = 177.5 kHz. No other combination of q_{CD} and γ values resulted in a better agreement between the experimental and calculated results. Interestingly, q_{CD} of 177.5 kHz is within the estimated values from the computations. When analysing the quadrupole splittings in the nematic phase, q_{CD} was fixed to the value of 177.5 kHz, while $P_2(\cos\gamma)$ was used as a free parameter. It came out that the best fit is achieved with $P_2(\cos\gamma)$ = 0.307583, which means that γ = 110.98°, *i.e.*, 1.4° larger than in the N_{TB} phase. Interestingly, ref. 12 reports that the principal ordering axis of biphenyl has tilted about 13° relative to the *para*-axis in the nematic phase. This is almost tenfold of the value observed here. It is, of course, possible that the tilt of 1.4° arises partly because the single order-parameter approximation for the biphenyl fragment works better in the N_{TB} phase than in the N phase. As discussed above, the relative contribution of the biaxial order parameter is twofold in the N phase as compared to that in the N_{TB} phase. The temperature dependence of the conical angle derived from the mean of the ^{2}H quadrupole splittings is displayed in Fig. 5 together with ^{129}Xe NMR and birefringence results. The conical angle as determined from the ^{2}H quadrupole splittings can be described using the following equation:

$$\theta(T) = 36.69 \times \left(1 - 0.998 \times \frac{T}{T_{N-N_{TB}}}\right)^{0.1762}, \qquad (8)$$

where $T_{N-N_{TB}}$ is the N–N_{TB} phase transition temperature, 374.4 K, in the present case.

^{129}Xe linewidth and activation energy

Fig. 6 shows the width of ^{129}Xe resonance peak as a function of temperature in CB7CB-D_4. The linewidth increases abruptly when approaching the phase transitions from the high-temperature side. Interestingly, the ^{2}H NMR spectrum of CB7CB-D_4 does not display a ^{2}H linewidth behaviour like that of xenon at the phase transitions.[38] Furthermore, for ^{129}Xe, the steep increase of the linewidth starts at a much higher temperature than in the case of ^{2}H. Upon lowering the temperature, a further increase of the ^{129}Xe linewidth takes place in the N_{TB} phase at about 359 K. Below this temperature, $\nu_{1/2}$(Xe) increases exponentially. A least-squares fit of the natural logarithm of the Arrhenius function (assuming that the activation energy E_A is independent of temperature)

$$\nu_{1/2}(\mathrm{Xe}) = a\mathrm{e}^{\frac{E_A}{RT}}, \qquad (9)$$

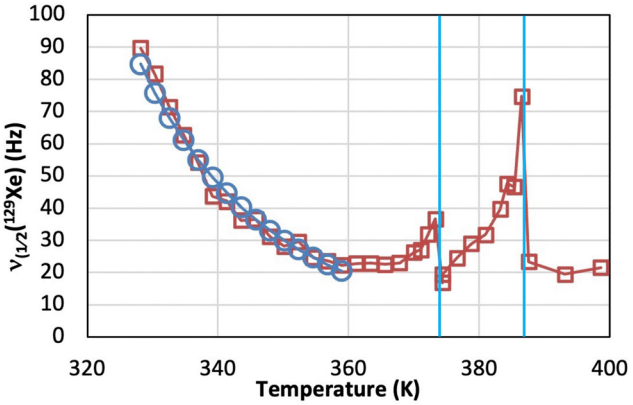

Fig. 6 Experimental and calculated linewidth $\nu_{1/2}(^{129}\mathrm{Xe})$ in the N_{TB} phase. The solid blue line is the least-squares fit of the experimental point to the Arrhenius law, in the N_{TB} phase. Phase transitions are indicated by vertical lines. Note: $\nu_{1/2}(^{129}\mathrm{Xe})$ = 2.80 Hz in the gas phase. The red squares and blue circles denote experimental and calculated points, respectively.

i.e., of the function

$$\ln \nu_{1/2}(\mathrm{Xe}) = \ln a + \frac{E_A}{RT} \qquad (10)$$

to the experimental data, results in $\ln a = -12.08 \pm 0.67$, and E_A = 45.08 ± 1.9 kJ mol^{-1}. Using eqn (9),

$$\nu_{1/2}(\mathrm{Xe}) = 5.644 \times 10^{-6}\mathrm{e}^{\frac{5422\ \mathrm{K}}{T}}\ \mathrm{Hz}. \qquad (11)$$

Linewidth at the phase transitions

As shown in Fig. 6, $\nu_{1/2}(^{129}\mathrm{Xe})$ increases steeply at both phase transitions, when approaching from the high-temperature side. After the transitions, $\nu_{1/2}(^{129}\mathrm{Xe})$ narrows exponentially back towards the same value as in the bulk isotropic phase, *ca.* 21 Hz. The N phase must be cooled by *ca.* 30 K and the N_{TB} phase by *ca.* 20 K from their respective phase transition temperatures, before the ^{129}Xe linewidth again approaches the isotropic value, or the value just before the phase transition. Fig. 7 (top) shows least-squares fits of function (12) to the experimental data leading to the mentioned values:

$$\nu_{1/2}(^{129}\mathrm{Xe}) = a + b\exp[c/(T - T_{PT})], \qquad (12)$$

where T_{PT} is either the I–N or N–N_{TB} phase transition temperature. Fig. 7 (bottom) displays the linewidth after removing the distributions at the phase transitions.

The values of the adjustable parameters in eqn (12) are given in Table 3.

The ^{129}Xe linewidth as a function temperature in CB7CB can now be presented in the form

$$\nu_{1/2}(^{129}\mathrm{Xe}) = \begin{cases} 21.46\ \mathrm{Hz}; & 359\ \mathrm{K} \le T < 390\ \mathrm{K} \\ 5.64 \times 10^{-6}\mathrm{e}^{\frac{5422\ \mathrm{K}}{T}}\ \mathrm{Hz}; & T \le 359\ \mathrm{K}. \end{cases} \qquad (13)$$

Spin–spin relaxation rate of ^{129}Xe

Neglecting possible effects from the inhomogeneity of the external magnetic field, the relaxation rate $1/T_2$ of ^{129}Xe is

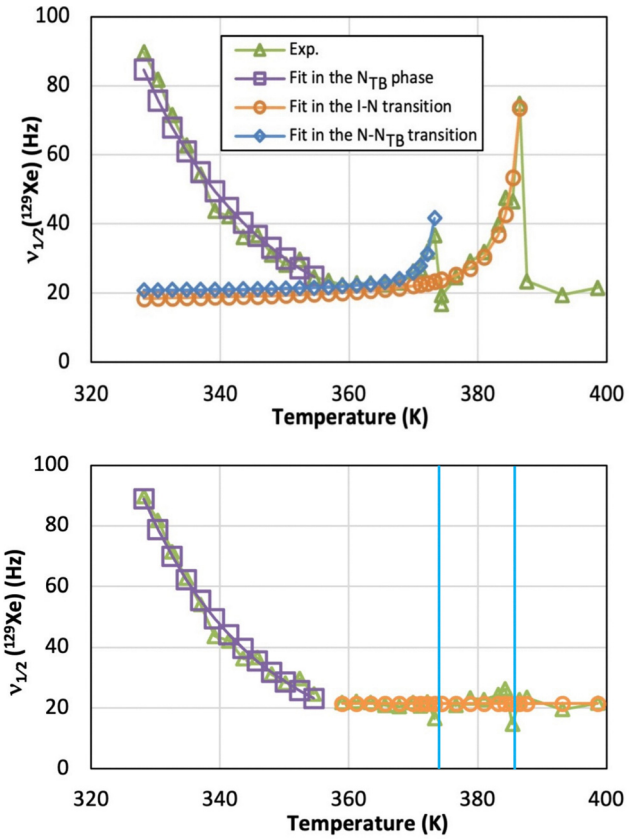

Fig. 7 (top) Least-squares fit of function (12) to experimental ^{129}Xe linewidths at the low-temperature sides of the phase transitions. It is seen that the minimum linewidth is *ca.* 21 Hz. (bottom) ^{129}Xe linewidth, $\nu_{1/2}$, when the distributions in the vicinity of the phase transitions are subtracted. The vertical lines indicate phase transition temperatures. Average linewidth equals 21.46 Hz between 359 and 398 K.

Table 3 Values of the parameters *a*, *b* and *c* in eqn (12)[a]

Phase transition	T_{PT} (K)	*a* (Hz)	*b* (Hz)	*c* (K)
I···N	387.1	78.5	−61.6	1.529
N···N$_{TB}$	374.4	163.3	−143.0	0.178

[a] Note: temperature was decreased slowly from the isotropic phase.

obtained from the linewidth:

$$\frac{1}{T_2} = \pi\nu_{1/2}. \tag{14}$$

It appears that $1/T_2$ (^{129}Xe) is linearly dependent upon the ratio of the rotational viscosity of CB7CB[39] and temperature, η/T, within the temperature range [328 K, 359 K]:

$$\frac{1}{T_2(^{129}\mathrm{Xe})} = c \times \frac{\eta}{T} + d, \tag{15}$$

where c = 43 174.08 K Pa^{-1} s^{-2} and d = 7.10168 s^{-1}. The dependence is shown in Fig. 8, while Fig. 9 displays $1/T_2$ (^{129}Xe) as a function of temperature within the above-mentioned temperature range.

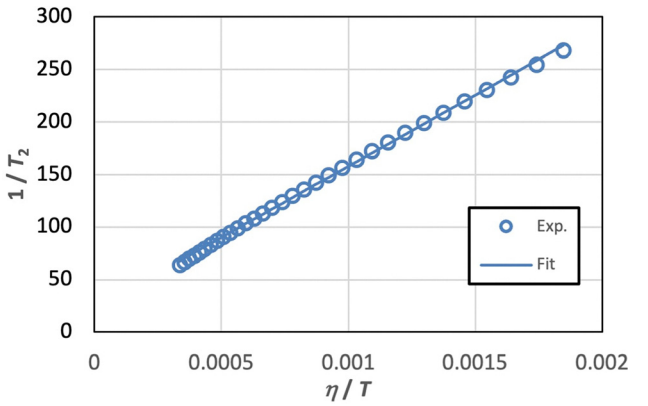

Fig. 8 $1/T_2$ (^{129}Xe) as a function of η/T, where η is the rotational viscosity of CB7CB and T is temperature.

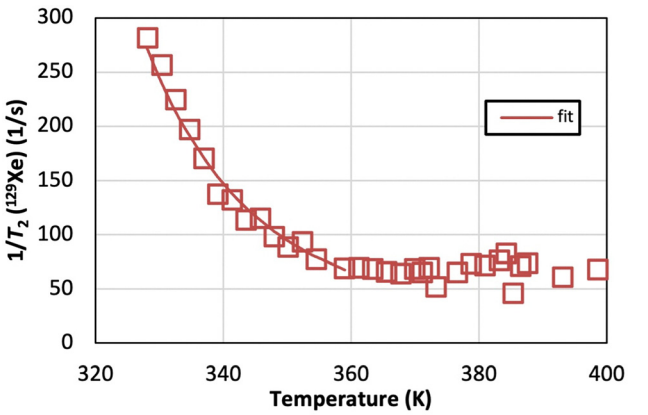

Fig. 9 $1/T_2$ (^{129}Xe) as a function of temperature. The solid line is from eqn (15).

According to the Stokes–Einstein–Debye model,[40] the rotational correlation time is linearly related to η/T:

$$\tau_c = \frac{V}{k_B}\frac{\eta}{T}, \tag{16}$$

where η is the rotational viscosity of CB7CB[39] and k_B is Boltzmann constant. For the calculation of τ_c, the molecular volume should be known. Use of the radius of gyration around the long axis of the molecule, 2.38 Å, of CB7CB results in $V = 5.649 \times 10^{-29}$ m^3, which is comparable to the polarizability volume of 428.78 Bohr^3 = 6.354×10^{-29} m^3, calculated at the presently applied level of theory. The temperature dependence of τ_c is illustrated in Fig. 10. Obviously, $1/T_2$ is directly proportional to τ_c.

When dealing with the relaxation of ^{129}Xe one must consider two mechanisms: (1) dipolar interaction of ^{129}Xe with the protons in CB7CB-D$_4$[41] and (2) ^{129}Xe shielding anisotropy.[42] We consider first the latter case.

The spin–spin relaxation rate due to shielding anisotropy is described by[42]

$$\frac{1}{T_{2(\mathrm{CSA})}} = \frac{1}{45}\gamma_{\mathrm{Xe}}{}^2 B_0{}^2 \Delta\sigma_{\mathrm{Xe}}{}^2 \tau_c \left[4 + \frac{3}{1+\omega_{\mathrm{Xe}}{}^2\tau_c{}^2}\right], \tag{17}$$

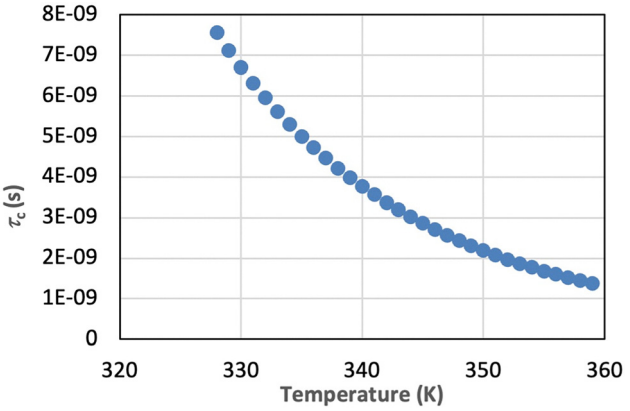

Fig. 10 Rotational correlation time of CB7CB as a function of temperature in the temperature range [328 K, 359 K].

where γ_{Xe} is the gyromagnetic ratio of xenon-129, B_0 is the magnetic flux density (14.07 T in the present case), and $\Delta\sigma_{Xe}$ is the shielding anisotropy. This anisotropy value is the result of the least-squares fit of the ^{129}Xe shielding to the function in eqn (5). It appears that the anisotropy is the same in the N and N_{TB} phases, *i.e.*, −47 ppm. The shielding anisotropy of ^{129}Xe arises from the deformation of its electron distribution due to the anisotropic environment. In other words, xenon experiences different interactions with the CB7CB molecules along different directions. Consequently, a plausible conclusion is that the correlation time in eqn (17) is the same as (or at least strongly related to) that for $1/T_2$ (^{129}Xe), shown in Fig. 10. It appears that $1/T_2$ (CSA) is directly proportional to τ_c at low temperatures and is negligibly small compared to the total $1/T_2$.

Obviously, the dominant relaxation mechanism is ^{129}Xe–^{1}H dipole–dipole interaction. As discussed, for example, in ref. 41, analytical treatment of the problem leads to complex time-correlation and spectral density functions. However, when dealing with the effect of diffusion, the translational diffusion correlation time can be presented in a simple form

$$\tau_c = \frac{d^2}{D_{CBXe}}, \tag{18}$$

where $D_{CBXe} = D_{CB7CB} + D_{Xe}$ is the mutual self-diffusion constant of the interacting species and d is the distance of closest approach between the spins. Here, D_{CB7CB} is the diffusion constant of CB7CB and D_{Xe} that of xenon. Both diffusion tensors are anisotropic. For example, the anisotropy of the CB7CB diffusion tensor, $D_{\parallel}/D_{\perp}$, is in the range of 1.5 to 3.2[43] while that of xenon-129 is typically below 1.[44,45] The self-diffusion coefficient of CB7CB-D_4 in the direction of the director/helix axis appears to be *ca.* 2 orders of magnitude smaller[43] than the typical values of ^{129}Xe in conventional liquid crystals, being of the order of 10^{-10}–10^{-9} m^2 s^{-1}.[7,44] Consequently, the Xe self-diffusion coefficient can be argued to dominate in eqn (18). If one assumes that $d \approx 3.5$ Å,[46] τ_c appears to be of the order of 10^{-11} s in the isotropic and nematic phases but *ca.* 10^{-10} s in the N_{TB} phase. However, d is obviously dependent upon temperature. Thus, when d increases (upon lowering the temperature), τ_c also increases.

The relaxation rate can be expressed as follows:[47]

$$\frac{1}{T_2} = \frac{1}{20}\left(\frac{\mu_0}{4\pi}\right)^2 \gamma_{Xe}{}^2\gamma_H{}^2\hbar^2\tau_c \sum_i^{26} \frac{1}{r_i^6}\left[4 + \frac{1}{1+(\omega_H-\omega_{Xe})^2\tau_c{}^2} + \frac{3}{1+\omega_{Xe}{}^2\tau_c{}^2} + \frac{6}{1+\omega_H{}^2\tau_c{}^2} + \frac{6}{1+(\omega_H+\omega_{Xe})^2\tau_c{}^2}\right]. \tag{19}$$

Here r_i is the distance between the xenon atom and the proton i, and ω_H and ω_{Xe} are the Larmor frequencies of ^{1}H and ^{129}Xe nuclei, respectively. Eqn (19), however, is only qualitatively correct as it assumes a constant internuclear distance. Furthermore, eqn (19) does not include the fact that one xenon-129 is surrounded by many CB7CB molecules, each carrying 26 protons. As discussed above, in the low-temperature part of the CB7CB data, *i.e.*, within the temperature range [328 K, 359 K], $1/T_2$ is directly proportional to the rotational correlation time of CB7CB. This means that the terms $(\omega_H - \omega_{Xe})^2\tau_c{}^2$, $\omega_{Xe}{}^2\tau_c{}^2$, $\omega_H{}^2\tau_c{}^2$ and $(\omega_H + \omega_{Xe})^2\tau_c{}^2$ in the denominators of the terms in eqn (19) are much larger than unity and the rotational diffusion of CB7CB dominates in the low-temperature part of the N_{TB} phase. In the high-temperature part of the N_{TB} phase and in the N phase, the situation is the opposite to the previous case, meaning that $(\omega_H - \omega_{Xe})^2\tau_c{}^2$, $\omega_{Xe}{}^2\tau_c{}^2$, $\omega_H{}^2\tau_c{}^2$ and $(\omega_H + \omega_{Xe})^2\tau_c{}^2$ are much smaller than unity. Still, $1/T_2$ remains directly proportional to the correlation time, but now to the diffusion correlation time.

Conclusions

We have applied ^{129}Xe NMR, quantum-chemical computations and earlier ^{2}H NMR data to address the structural and dynamic properties of the twist-bend nematic liquid crystal phase formed by the CB7CB molecules. The conical angle of the twist-bend nematic phase defines the nanoscale geometry and optical properties of the phase. It influences, for example, birefringence and electro-optical responses. Consequently, it is a very important property. Here, it was derived from the ^{129}Xe and ^{2}H NMR experiments. In the former case, temperature dependence of the chemical shift was utilized, while in the latter case quadrupole coupling was used. When using xenon-129 as an external chemical shift reference, it is necessary to apply the bulk susceptibility correction. The correction was calculated using the isotropic diamagnetic susceptibility calculated in this work as no experimental value could be found from the literature. For the diamagnetic anisotropy, two values were used: one from the present computations and one from experiments, the latter being *ca.* twofold. It is shown that in both cases the correction leads to an increase in the temperature dependence of the conical angle in the CB7CB-D_4 liquid crystal. The conical angle was also determined from the mean of the temperature-dependent ^{2}H quadrupolar splittings in the twist-bend nematic phase. In this case, it is necessary to assume that the orientational order of the biphenyl fragments can be described by a single order parameter. The temperature dependence of the conical angle derived from the susceptibility-corrected ^{129}Xe

shielding values agrees well with the one from the birefringence measurements in ref. 35.

When moving to low temperature, the ^{129}Xe linewidth increases rapidly at the low temperature part of the twist-bend nematic phase, the activation energy being 45.08 kJ mol^{-1}. The linewidth increases abruptly when approaching I–N and N–N_{TB} phase transitions from the high-temperature side and decays exponentially towards a value of *ca.* 21.5 Hz after the transitions. The transitions to this value need temperature decreases by *ca.* 30 K in the N phase and by *ca.* 20 K in the N_{TB} phase. When the contributions to the linewidth at phase transitions are removed, the linewidth (and spin–spin relaxation rate) appears practically insensitive to temperature variation in the isotropic and nematic phases and in the high temperature part of the N_{TB} phase. It is concluded that the self-diffusion of xenon-129 makes the principal contribution to the $1/T_2$ relaxation rate in the isotropic and nematic phases, while in the low-temperature N_{TB} phase the rotation of the CB7CB molecules becomes more crucial.

Author contributions

J. J.: conceptualization, general investigation, analysis of experimental data, and writing of the original draft. J. V.: quantum-chemical calculations and their analysis. Both authors contributed together to the reviewing/editing of the manuscript.

Conflicts of interest

There are no conflicts to declare.

Data availability

The data supporting this article have been included as part of the supplementary information (SI). Supplementary information: optimised structures of 5CB and CB7CB at different levels of theory, the computed magnetizability tensor data used in conformational averaging, and experimental ^{129}Xe chemical shifts and ^{2}H quadrupole splittings, which the analyses are based on, belong to earlier published data. See DOI: https://doi.org/10.1039/d5cp02069g.

Acknowledgements

The authors would like to thank P. Hilla (Oulu) for useful discussions. Financial support from the Academy of Finland (project 361326) and the Kvantum Institute of the University of Oulu is gratefully acknowledged. Computational resources were supplied by the CSC-IT Center for Science (Espoo, Finland).

References

1 D. Dunmur, *Crystals*, 2022, **12**, 309.
2 S. Ahola, P. Ingman, R. Laatikainen, J. Sinkkonen and J. Jokisaari, *J. Chem. Phys.*, 2018, **149**, 234901.
3 J. Jokisaari, A. M. Kantola, J. Lounila and L. P. Ingman, *Phys. Rev. Lett.*, 2011, **106**, 017801.
4 J. Jokisaari and J. Zhu, *Magn. Reson. Chem.*, 2014, **52**, 556.
5 J. Jokisaari, *Liq. Cryst.*, 2020, **47**, 15955.
6 J. Jokisaari, G. R. Luckhurst, B. Timimi, J. Zhu and H. Zimmermann, *Liq. Cryst.*, 2015, **42**, 708.
7 J. Ruohonen, M. Ylihautala and J. Jokisaari, *Mol. Phys.*, 2001, **99**, 711.
8 J. Lounila, O. Muenster, J. Jokisaari and P. Diehl, *J. Chem. Phys.*, 1992, **97**, 8977.
9 J. Jokisaari and P. Diehl, *Liq. Cryst.*, 1990, **7**, 739.
10 J. Jokisaari, P. Diehl and O. Muenster, *Mol. Cryst. Liq. Cryst.*, 1990, **188**, 189.
11 L. Longa and W. Tomczyk, *J. Phys. Chem. C*, 2020, **124**, 22761.
12 C. Greco, A. Ferrarini, G. R. Luckhurst, B. A. Timimi and H. Zimmermann, *Liq. Cryst.*, 2018, **45**, 2361.
13 M. Cestari, S. Diez-Berart, D. A. Dunmur, A. Ferrarini, M. R. de la Fuente, D. J. B. Jackson, D. O. Lopez, G. R. Luckhurst, M. A. Perez-Jubinho, R. M. Richardson, J. Salud, B. A. Timimi and H. Zimmermann, *Phys. Rev. E:Stat., Nonlinear, Soft Matter Phys.*, 2011, **84**, 031704.
14 P. K. Challa, V. Borshch, O. Parri, C. T. Imrie, S. N. Sprunt, J. T. Gleeson, O. D. Lavrentovich and A. Jakli, *Phys. Rev. E:Stat., Nonlinear, Soft Matter Phys.*, 2014, **89**, 060501.
15 C. Adamo and V. Barone, *J. Chem. Phys.*, 1999, **110**, 6158.
16 F. Weigend and R. Ahlrichs, *Phys. Chem. Chem. Phys.*, 2005, **7**, 3297.
17 TURBOMOLE V7.8.1 2024, a development of University of Karlsruhe and Forschungszentrum Karlsruhe GmbH, 1989–2024, TURBOMOLE GmbH, since 2007; available from https://www.turbomole.org.
18 E. Caldeweyher, C. Bannwarth and S. Grimme, *J. Chem. Phys.*, 2017, **147**, 034112.
19 D. Rappoport and F. Furche, *J. Chem. Phys.*, 2010, **133**, 134105.
20 M. J. Frisch, G. W. Trucks, H. B. Schlegel, G. E. Scuseria, M. A. Robb, J. R. Cheeseman, G. Scalmani, V. Barone, G. A. Petersson, H. Nakatsuji, X. Li, M. Caricato, A. V. Marenich, J. Bloino, B. G. Janesko, R. Gomperts, B. Mennucci, H. P. Hratchian, J. V. Ortiz, A. F. Izmaylov, J. L. Sonnenberg, D. Williams-Young, F. Ding, F. Lipparini, F. Egidi, J. Goings, B. Peng, A. Petrone, T. Henderson, D. Ranasinghe, V. G. Zakrzewski, J. Gao, N. Rega, G. Zheng, W. Liang, M. Hada, M. Ehara, K. Toyota, R. Fukuda, J. Hasegawa, M. Ishida, T. Nakajima, Y. Honda, O. Kitao, H. Nakai, T. Vreven, K. Throssell, J. A. Montgomery, Jr., J. E. Peralta, F. Ogliaro, M. J. Bearpark, J. J. Heyd, E. N. Brothers, K. N. Kudin, V. N. Staroverov, T. A. Keith, R. Kobayashi, J. Normand, K. Raghavachari, A. P. Rendell, J. C. Burant, S. S. Iyengar, J. Tomasi, M. Cossi, J. M. Millam, M. Klene, C. Adamo, R. Cammi, J. W. Ochterski, R. L. Martin, K. Morokuma, O. Farkas, J. B. Foresman and D. J. Fox, *Gaussian 16, Revision C.02*, Gaussian, Inc., Wallingford CT, 2016.
21 G. Babakhanova, Z. Parsouzi, S. Paladugu, H. Wang, Yu. A. Nastishin, S. V. Shiyanovskii, S. Sprunt and O. D. Lavrentovich, *Phys. Rev. E*, 2017, **96**, 062704.

22 P. W. Atkins and R. S. Freedman, *Molecular Quantum Mechanics*, Oxford University Press, Oxford, 5th edn, 2011.
23 A. Buka and W. H. de Jeu, *J. Phys.*, 1982, **43**, 361.
24 F. Neese, *Wiley Interdiscip. Rev.: Comput. Mol. Sci.*, 2018, **8**, e1327.
25 P. Perdew, K. Burke and M. Ernzerhof, *Phys. Rev. Lett.*, 1996, **77**, 3865–3868; P. Perdew, K. Burke and M. Ernzerhof, *Phys. Rev. Lett.*, 1997, **78**, 1396.
26 J. Vaara and Y. Hiltunen, *J. Chem. Phys.*, 1997, **107**, 1744.
27 A. M. Kantola, S. Ahola, J. Vaara, J. Saunavaara and J. Jokisaari, *Phys. Chem. Chem. Phys.*, 2007, **9**, 481.
28 G. R. Luckhurst, B. A. Timimi, N. J. Wells and H. Zimmermann, *Liq. Cryst.*, 2018, **45**, 1913.
29 B. Robles-Hernández, N. Sebastian, M. R. de la Fuente, D. O. López, S. Diez-Berart, J. Salud, M. B. Ros, D. A. Dunmur, G. R. Luckhurst and B. A. Timimi, *Phys. Rev. E:Stat., Nonlinear, Soft Matter Phys.*, 2015, **92**, 062505.
30 D. Buckingham and E. E. Burnell, *J. Am. Chem. Soc.*, 1967, **89**, 3341.
31 I. Haller, *Prog. Solid State Chem.*, 1975, **10**, 103.
32 J. Lounila, O. Münster, J. Jokisaari and P. Diehl, *J. Chem. Phys.*, 1992, **97**, 8977.
33 M. Ylihautala, J. Lounila and J. Jokisaari, *Chem. Phys. Lett.*, 1999, **301**, 153.
34 C. Jameson, A. K. Jameson and S. M. Cohen, *J. Chem. Phys.*, 1975, **59**, 4540.
35 M. R. Tuchband, M. Shuai, K. A. Graber, D. Chen, C. Zhu, L. Radzihovsky, A. Klittnick, L. Foley, A. Scarbrough, J. H. Porada, M. Moran, J. Yelk, J. B. Hooper, X. Wei, D. Bedrov, C. Wang, E. Korblova, D. M. Walba, A. Hexemer, J. E. Maclennan, M. A. Glaser and N. A. Clark, *Crystals*, 2024, **14**, 583.
36 C. Meyer, G. R. Luckhurst and I. Dozov, *J. Mater. Chem. C*, 2015, **3**, 318.
37 J. W. Emsley, M. Lelli, A. Lesage and G. R. Luckhurst, *J. Phys. Chem. B*, 2013, **117**, 6547.
38 G. R. Luckhurst and B. Timimi, *private communication*.
39 K. Merkel, A. Kocot, C. Welch and G. H. Mehl, *Phys. Chem. Chem. Phys.*, 2019, **21**, 22839.
40 P. Debye, *Polar Molecules*, The Chemical Catalog Company, 1929.
41 J. Kowalewski and L. Mäler, *Nuclear spin Relaxation in Liquids. Theory, Experiments and Applications*, CRC Press, 2nd edn, 2019, ch. 3.
42 J. S. Blicharski, *Z. Naturforsch.*, 1972, **27a**, 1456.
43 M. Cifelli, V. Domenici, S. V. Dvinskikh, G. R. Luckhurst and B. A. Timimi, *Liq. Cryst.*, 2016, **44**, 1254292.
44 J. Ruohonen and J. Jokisaari, *Phys. Chem. Chem. Phys.*, 2001, **3**, 3208.
45 H. W. Long, M. Luzar, H. C. Gaede, R. G. Larsen, J. Kritzenberger and A. Pines, *J. Phys. Chem.*, 1995, **99**, 11989.
46 J. Vaara, J. Jokisaari, T. T. Rantala and J. Lounila, *Mol. Phys.*, 1994, **82**, 13.
47 I. Solomon, *Phys. Rev.*, 1955, **99**, 559.

